As shown in Figure 4f, some branched nanotubes with a 90° angle between branches could be also found in Sample 3. We believe that these branched nanotubes have originated from some branched Al_4O_4C nanowires (Figs. 2d,e). High-resolution TEM observations and ED analysis prove that alumina nanotubes had remained single crystals during the oxidation treatment. Representative HRTEM micrographs and the corresponding ED patterns of the individual nanotubes are displayed in Figures 4g,h. The axial directions are along the [001] or [101] orientations of α-Al_2O_3.

To sum up, single-crystalline Al_4O_4C nanowires were synthesized by a simple vapor–solid process based on a high-temperature reaction. Single-crystalline α-Al_2O_3 nanotubes were then successfully prepared from these Al_4O_4C nanowires using a two-step reaction method. Three-layer C–Al_2O_3–C nanotubes, appearing at the initial reaction stage, may be particularly useful in nanoelectronics. Most importantly, we envisage that pure single-crystalline α-Al_2O_3 ceramic nanotubes may find novel high-temperature applications in nanotechnology due to their unmatched refractory properties.

Experimental

The Al_4O_4C nanowires were synthesized in a JEOL vertical high-frequency induction furnace in which a rod-like graphite inductor acted as the heater. A tubular alumina crucible, 20 mm in outer diameter and 100 mm in length, was inserted into the central space (size: 20 mm × 100 mm) of the graphite heater. This ensured close physical contact between alumina and graphite. After the chamber was evacuated to 2.5×10^{-3} Pa, the graphite heater was rapidly heated to 1550–1600 °C and held at that temperature for over 1 h. After the whole chamber cooled down to room temperature, a thick layer of light-green-colored powder (Sample 1) was collected from the upper outer surface of the alumina crucible. The lower part of the alumina crucible was found to be heavily eroded. The process described above leads to the high-yield production of pure Al_4O_4C nanowires, ~250 mg in weight per run (see Supporting Information, Figure S1). This enabled us to carry out various characterizations as well as further experiments. In order to produce C–Al_2O_3–C nanotubes, the prepared Al_4O_4C nanowires were put into a BN crucible placed at the bottom of the cylindrical graphite heater. Heating was performed in the same induction furnace described above. When the chamber was evacuated down to 100 Pa, the pump was stopped. This ensured some residue of low-pressure air (100 Pa) in the chamber. Then, the sample was heated to 1200 °C and held at that temperature for 30 min. Heating led to the generation of CO gas due to the reaction between the residual air and the graphite heater. After this treatment, the sample (Sample 2) color appeared to be dark gray. To obtain pure Al_2O_3 nanotubes (Sample 3), Sample 2 was oxidized in air at 800 °C for 20 min. X-ray diffraction (XRD) patterns of the nanostructures were recorded on a RINT2200 X-ray diffractometer using standard Cu Kα radiation. The morphology of the nanostructures was observed by scanning electron microscopy (SEM) using a JSM-6700F SEM. Detailed structural transmission electron microscopy (TEM) characterization was performed on a JEM-3000F field-emission TEM operated at 300 kV. Energy dispersion X-ray (EDX) spectroscopy of chemical composition microanalysis was carried out using an EDX spectrometer attached to the TEM.

Received: August 24, 2004
Final version: February 28, 2005

[1] J. Goldberger, R. R. He, Y. F. Zhang, S. W. Lee, H. Q. Yan, H. J. Choi, P. D. Yang, *Nature* **2003**, *422*, 599.
[2] J. Q. Hu, Y. Bando, Z. W. Liu, J. H. Zhan, D. Golberg, T. Sekiguchi, *Angew. Chem. Int. Ed.* **2004**, *43*, 63.
[3] Y. B. Li, Y. Bando, D. Golberg, Z. W. Liu, *Appl. Phys. Lett.* **2003**, *83*, 999.
[4] Y. B. Li, Y. Bando, D. Golberg, *Adv. Mater.* **2003**, *15*, 581.
[5] Y. B. Li, Y. Bando, D. Golberg, *Adv. Mater.* **2003**, *15*, 1294.
[6] R. G. Munro, *J. Am. Ceram. Soc.* **1997**, *80*, 1919.
[7] T. Yanagishita, M. Sasaki, K. Nishio, H. Masuda, *Adv. Mater.* **2004**, *16*, 429.
[8] J. S. Lee, B. Min, K. Cho, S. Kim, J. Park, Y. T. Lee, N. S. Kim, M. S. Lee, S. O. Park, J. T. Moon, *J. Cryst. Growth* **2003**, *254*, 443.
[9] J. Hwang, B. Min, J. S. Lee, K. Cho, M. Y. Sung, M. S. Lee, S. Kim, *Adv. Mater.* **2004**, *16*, 422.
[10] a) L. Pu, X. M. Bao, J. P. Zou, D. Feng, *Angew. Chem. Int. Ed*. **2001**, *40*, 1490. b) J. P. Zou, L. Pu, X. M. Bao, D. Feng, *Appl. Phys. Lett*. **2002**, 80, 1079. c) Y. F. Mei, X. L. Wu, X. F. Shao, G. C. Siu, X. M. Bao, *Europhys. Lett.* **2003**, *62*, 595.
[11] Z. L. Xiao, C. Y. Han, U. Welp, H. H. Wang, W. K. Kwok, G. A. Willing, J. M. Hiller, R. E. Cook, D. J. Miller, G. W. Crabtree, *Nano Lett.* **2002**, *2*, 1293.
[12] Y. J. Zhang, J. Liu, R. R. He, Q. Zhang, X. Zhang, J. Zhu, *Chem. Phys. Lett.* **2002**, *360*, 579.
[13] B. C. Satishkumar, A. Govindaraj, E. M. Vogl, L. Basumallick, C. N. R. Rao, *J. Mater. Res.* **1997**, *12*, 604.
[14] D. Kuang, Y. Fang, H. Liu, C. Frommen, D. Fenske, *J. Mater. Chem.* **2003**, *13*, 660.
[15] H. C. Lee, H. J. Kim, S. H. Chung, K. H. Lee, H. C. Lee, J. S. Lee, *J. Am. Chem. Soc.* **2003**, *125*, 2882.
[16] C. J. Deng, P. Yu, M. Y. Yau, C. S. Ku, D. H. L. Ng, *J. Am. Ceram. Soc.* **2003**, *86*, 1385.
[17] X. S. Fang, C. H. Ye, X. S. Peng, Y. H. Wang, Y. C. Wu, L. D. Zhang, *J. Mater. Chem.* **2003**, *13*, 3040.
[18] S. Zhang, A. Yamaguchi, *J. Ceram. Soc. Jpn.* **1996**, *104*, 393.

Routes to Grow Well-Aligned Arrays of ZnSe Nanowires and Nanorods**

By *Xitian Zhang*, *Zhuang Liu*, *Quan Li*, *Yeepan Leung*, *Kitman Ip*, and *Suikong Hark**

A variety of semiconductor nanowires and nanorods can now be grown directly on many kinds of substrates by several methods.[1,2] Among the many methods, chemical vapor deposition (CVD) enjoys a long history and great popularity be-

[*] Prof. S. Hark, Prof. X. Zhang,[+] Z. Liu, Prof. Q. Li, Y. Leung, K. Ip
Department of Physics, The Chinese University of Hong Kong
Shatin, Hong Kong (P.R.China)
E-mail: skhark@phy.cuhk.edu.hk
[+] On leave from the Department of Physics, Harbin Normal University, P.R.China.

[**] The work in this paper was partially supported by grants from the Research Grants Council of the Hong Kong Special Administrative Region, China (Project No. CUHK 4247/01P and 401003) and a CUHK Direct Grant 2060277.

 DOI: 10.1002/adma.200401891

ADVANCED MATERIALS

cause of its ease of operation. However, the majority of nanowires obtained by CVD tend to result in "weed" growth, in which there is no order in position or orientation. In the few exceptional cases where the crystal habit and anisotropy of the crystal structure may be exploited, acicular growth results in columns of nanowires or nanorods on substrates.[3–9] When there is no innate tendency to grow along a particular direction, such as for crystals belonging to the cubic system, it is more difficult to obtain oriented growth by CVD. However, this can be easily overcome by epitaxial-growth techniques. Epitaxially grown zinc-blende-structured nanowires have been achieved by molecular-beam epitaxy on GaAs (100) and GaP (111) substrates.[10,11] Highly aligned nanorods of GaAs and InAs have been grown on GaAs substrates by metal–organic chemical vapor deposition (MOCVD).[12,13] The obtained nanorods tend to be short, without a very large aspect ratio, and have a conical shape. Because of a lack of group II–VI substrates, group II–VI epitaxy is traditionally achieved with group III–V substrates. However, group II–VI semiconductors are more ionic in character than group III–V ones. This large difference in the ionicities of the two materials has been considered to be undesirable and has often been implicated as one of the sources of difficulty in obtaining group II–VI epilayers as good as group III–V ones. It would be interesting to know if the adverse effects of the differences in ionicities also extends to group II–VI nanowires and nanorods, and especially to their orientations. We have previously shown that long ZnSe nanowires and nanoribbons can be grown on Si substrates using MOCVD,[14] but the dissimilar crystal structures of the two materials result in growth without a preferred orientation. In this article, we show that it is possible to control the orientation of the ZnSe nanowires and nanorods on GaAs substrates, with or without a catalyst, using MOCVD.

Under the growth conditions studied, we found that very few ZnSe nanowires appeared on GaAs, even with gold as a catalyst. Previous studies had found it difficult to grow nanowires of GaAs and InAs on GaAs (111)A and (211)A substrates.[12] However, the nanowires could be readily grown if a high-quality, thin ZnSe epilayer was first deposited. The structure of the epilayers was assessed by high-resolution X-ray diffraction (HRXRD). Figure 1 shows a representative HRXRD rocking curve of the ZnSe epilayer on a GaAs (100) substrate. The narrow (004) peak and prominent Pendellosung fringes demonstrate that the epilayer is of a quality on par with the state of the art. Monoatomic surface steps were also observed by atomic force microscopy. Other epilayers on different GaAs surfaces were of comparable quality. The thickness of the epilayers was estimated to be ~200 nm from the interference fringes of the reflectance spectra. Under microscopic observation, the nanowires and nanorods were found to possess a high degree of orientational order on the substrates; their orientations are determined by their direction of growth and the nature of the surface of GaAs. X-ray diffraction (XRD) of the nanowires shows they have the zinc blende structure, regardless of which surface they grow on.

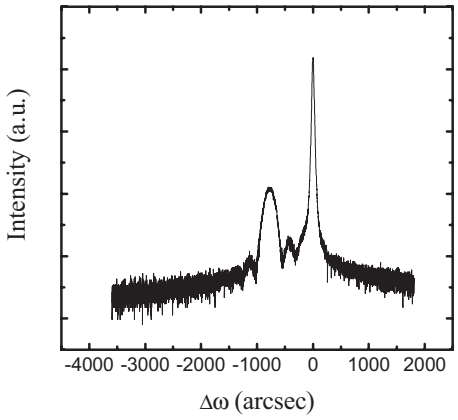

Figure 1. X-ray rocking curve of a ZnSe epilayer grown on a GaAs (100) substrate. The (004) diffraction peak of the epilayer is at $\Delta\omega = -789$ arcsec relative to that of the substrate at $\Delta\omega = 0$.

Figure 2 shows a typical XRD pattern of the nanowires grown on a GaAs (211)A substrate. The diffraction peaks can be indexed to the cubic structure of bulk ZnSe, with a cell constant of $a = 5.667$ Å (Joint Committee on Powder Diffraction Standards [JCPDS] file No. 05-0522), within experimental error. We note that the relative intensities of the peaks in the XRD pattern deviate significantly from those of random powder patterns; the stronger-than-usual (422) peak also reflects the X-ray texture of the nanowires.

The textures of the nanowires grown on different GaAs surfaces were examined by scanning electron microscopy (SEM). The plan-view SEM images in Figure 3 shows the apparent degree of orientational order of the nanowires and their directions of projection on the surface. With very few deviations, on the (100) surface the projected directions are preferentially along the four possible directions of <001> (Fig. 3a); on (211)A, they are mostly along either $[01\bar{1}]$ and $[0\bar{1}1]$ (Fig. 3b); and on (111), along $[11\bar{2}]$, $[1\bar{2}1]$, and $[\bar{2}11]$ (Fig. 3c). The images indicate that the ZnSe nanowires on GaAs grow along a

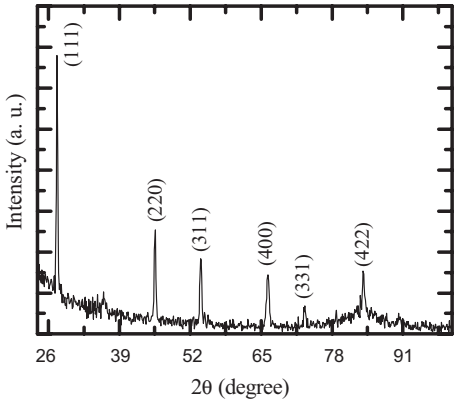

Figure 2. X-ray diffraction pattern of ZnSe nanowires grown on a GaAs (211)A substrate. The (422) peak of the nanowires is superimposed upon that of the substrate. The substrate had been slightly tilted to suppress the otherwise very intense diffraction; but still a weak remnant remains.

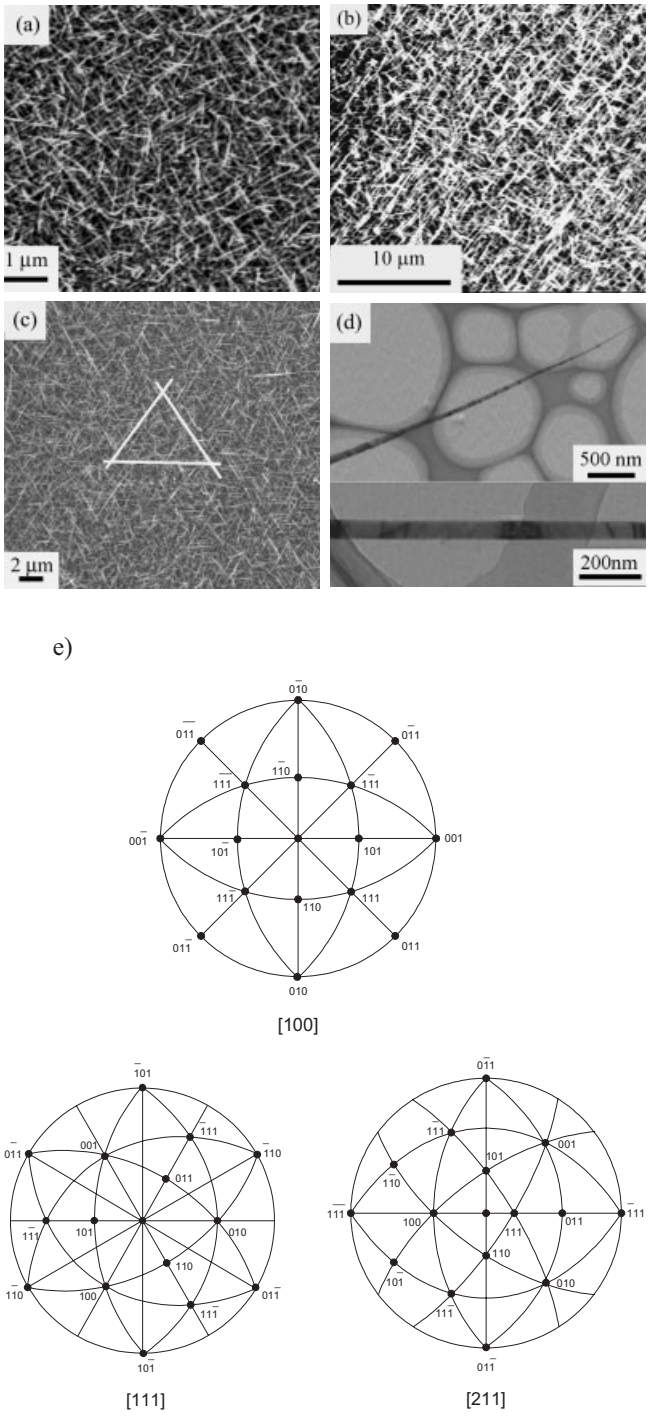

Figure 3. Images of the nanowires grown on various GaAs surfaces and the corresponding stereographs, showing the geometrical relationships among the surface normal, the growth directions, and the projections on the surface. Plan-view SEM images of the nanowires on GaAs a) (100), b) (211)A, and c) (111)A surfaces. Preferential alignment of the nanowires can be seen. The white triangle in (c) is a guide for the eye showing the preferred three-fold symmetry. d) Low-magnification transmission electron microscopy images of ZnSe nanowires, and e) [100], [111], and [211] pole stereographic projection diagrams of a cubic crystal.

special direction. By rotating the substrates about their surface normal and tilting about suitably chosen axes, we could observe the nanowires from different perspectives and determine, by geometrical projections, the angle θ they make with the normal. This angle is about 45° on (100), 30° on (211)A, and 38° on (111)A. Examination of the corresponding pole stereographs in Figure 3e readily identifies that nanowires growing along any of the physically identical <110> directions would produce the observed projections and angles. A comparison of the observed and calculated projections and angles θ of the nanowires is provided in Table 1. We note that certain directions of growth, theoretically possible according to the stereographs, are not observed. For example, on the (111)A surface, there are a total of six more directions of the <01$\bar{1}$> set, all lying on the equatorial plane, that are physically

Table 1. Projection directions and experimental (θ_{exp}) and calculated (θ_{cal}) angles of nanowires growing along <110> and <111>.

Sample	Substrate	Tilting Axis	θ_{exp} (±2°)	θ_{cal}	Projection Direction
Nanowires	(100)	<001>	45°	45°	[001][00$\bar{1}$][0$\bar{1}$0][010]
Nanowires	(211)A	<01$\bar{1}$>	30°	30°	[0$\bar{1}$1] [01$\bar{1}$]
Nanowires	(111)A	<$\bar{2}$11>	38°	35.26°	[11$\bar{2}$] [$\bar{2}$11] [1$\bar{2}$1]
Nanorods	(100)	<0$\bar{1}$1>	56°	54.74°	[0$\bar{1}$1] [01$\bar{1}$]
Nanorods	(100)	<011>	15.9°	15.80°	[011][0$\bar{1}\bar{1}$]

equivalent to the three observed. We suspect that growth along these directions, which would require the nanowires to be flat on the substrate, was stunted by obstruction by the neighboring nanowires. A similar argument applies to the (211)A surface, where observations show that nanowires growing along directions with a small θ are more favored.

The morphologies of the nanowires were examined by transmission electron microscopy (TEM) and are shown in Figure 3d. The nanowires typically average ~10 μm in length and about 80 nm in diameter. Some of the wires gradually taper towards a very sharp end, while others are more uniform along their length. Gold was not found at the tip or the base of the nanowires, casting doubt about the suitability of the vapor–liquid–solid (VLS) mechanism in explaining the rise of nanowires from epilayers of the same material. The nanowires probably grow via a vapor–solid mechanism, with small gold particles providing the nucleation sites. Gold also affects the direction of growth, as we will show later; without it, ZnSe nanowires tend to grow along the <111> directions. Once nucleated, epitaxy, coupled with the preferred direction of growth, gives rise to the orientational order of the nanowires. The direction of growth was also examined by high-resolution transmission electron microscopy (HRTEM). The lattice image of Figure 4 demonstrates the single-crystalline nature and the <110> growth direction of a nanowire.

More interestingly, well-oriented ZnSe nanorods can be directly grown on a ZnSe epilayer, without any catalyst. Fig-

ADVANCED MATERIALS

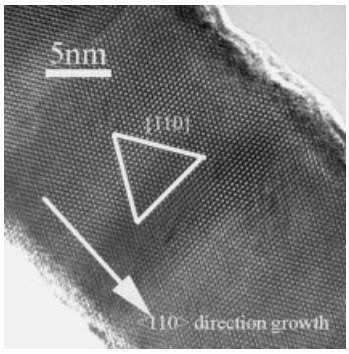

Figure 4. A HRTEM lattice image of a ZnSe nanowire along the [111] zone axis, showing its {110} planes and <110> growth direction.

ure 5 shows the SEM images of these nanorods from the same region on a GaAs (100) substrate from two different perspectives. We differentiate the nanorods from the nanowires mainly by their different aspect ratios. Figure 5 shows that most of the well-oriented nanorods make a 55.9° angle with the surface normal and have a projection onto the (100) plane parallel to [01$\bar{1}$]. A few nanorods are found to grow almost normal to the substrate, and tend to be not as well aligned. Geometrical analyses of Figures 5a,b indicate that most nanorods grow along <111>. There are several notable differences between the nanorods grown without catalyst and nanowires grown with gold as a catalyst. Nanowires are found in higher densities, with the directions of growth about evenly distributed among all four possible <011> directions, in contrast to

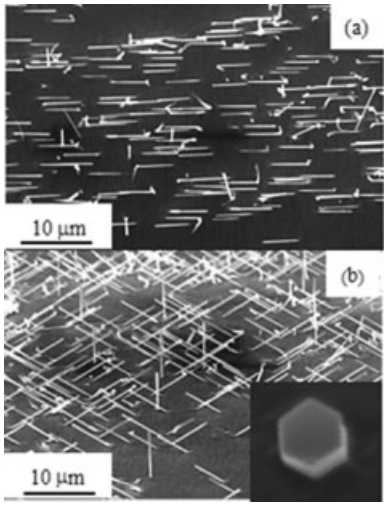

Figure 5. SEM images of ZnSe nanorods epitaxially grown on a GaAs (100) substrate: a) a plan view showing that their projections are mostly along [0$\bar{1}$1] or [01$\bar{1}$] directions; and b) a perspective view, at 60° tilt, of the nanorods in (a). The inset in (b) shows the view of a nanorod from the tip down in a SEM, showing its hexagonal cross-section and the orientation of the bounding surfaces on the substrate. The diameter of the nanorod is about 150 nm.

nanorods, which tend to grow preferentially along two of the four possible <111> directions. The morphology of the nanorods is also different from that of the nanowires. The former have regular hexagonal cross-sections, with diameters of about 150 nm. The ~10 μm long rods are bound by six {110} faces, which can be inferred from their orientations with respect to the substrate (Fig. 5b, inset). These differences suggest that the growth mechanisms of the nanorods and nanowires are different. In both cases, growth is preceded by nucleation. The nanorods appear to have nucleated at the emergent points of dislocations in the epilayer, while the nanowires have nucleated at small gold particles. The observations that most nanorods seem to grow from points on the crosshatches suggests that they probably share a common origin. The appearance of crosshatches on epilayers has been shown to be caused by misfit dislocations near the epilayer–substrate interface.[15] Associated with the misfit dislocations are threading dislocations that go through the epilayer and terminate on its surface. Classical crystal-growth theories have shown that under conditions of low supersaturation, nucleus formation is mostly facilitated at the sites of the dislocation outcrops.[16] For zinc-blende-structured epilayers grown on (100) substrates, the majority of the crosshatches run parallel to [0$\bar{1}$1], with a few parallel to the orthogonal [011] direction.[17] We note that the crosshatches are only observed in high-quality epilayers that are thicker than a critical value, determined mostly by the lattice mismatch.[15] Epilayers of lesser quality tend to contain too high of a density of dislocations and other defects to allow them to develop. The low density and preferred [0$\bar{1}$1] projection of the nanorods are both consistent with the nature of the crosshatches.[18] ZnO could also be grown without any introduced catalyst. It is believed that Zn droplets formed during growth can play the role of a catalyst.[19] We note that the [111] growth direction of the zinc-blende-structured ZnSe nanorods is related to the [0001] growth direction of wurtzite-structured ZnO. It is perhaps also possible that Zn droplets similarly act as a self-catalyst in the growth of the ZnSe nanorods. The high density and changed morphology of the nanowires are affected by the presence of gold coated on the epilayer. Apparently, small gold particles are more effective as nucleation sites and there are far more of them than the dislocation emergent points. The presence of impurities, such as gold, even at a very low concentration, is known to have a strong effect on the habit of a crystal. The impurity is often thought to affect the surface energies, and as a result, the morphology of the crystal. For ZnSe nanowires, gold has been suggested as a cause for their preferred <110> direction of growth.[10] Without gold modifying the surface energies, the nanorod grows in such a way that it leaves behind only the lowest-energy bounding {110} surfaces, which are also well-known as the easy fracture planes of zinc-blende-structured binary compound semiconductors.

Not using a catalyst has its advantages as far as possible contamination and unintended doping are concerned. Many metallic catalysts used in growing semiconducting nanowires are also known to form deep-level defects in them. For exam-

ple, gold is known to be a trap center in Si and GaAs, as is silver in ZnSe. Not having a catalyst seems to result in a lower yield of nanowires, but this is not really an important issue in device fabrication—controlling exactly where they grow is far more important. In any case, the density of nanowires might be adjusted by changing the density of dislocations and their outcrops. Compared with the weed-growth mode, our routes of growing oriented nanowires and nanorods and of controlling their alignment on the substrate looks more promising for the fabrication of nanodevices. However, the electronic and optical properties of the resulting materials also need to be examined before they can be considered to be useful.

Figure 6a shows a representative photoluminescence (PL) spectrum of ZnSe nanowires on a GaAs (100) substrate. Spectra of nanowires grown on other surfaces are similar. The spectrum clearly displays a sharp and strong near-band-edge (NBE) peak at 2.687 eV. The width of the peak is only about

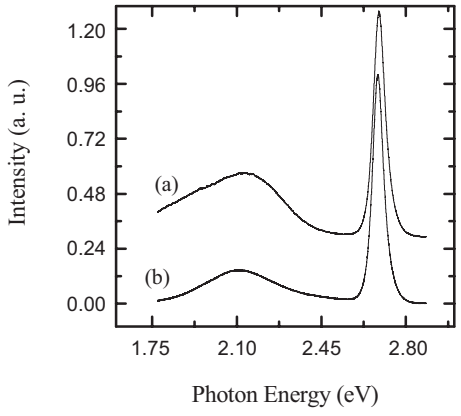

Figure 6. Room-temperature PL spectra of a) nanowires and b) nanorods.

53 meV, about the same as would be expected from thermal broadening alone. A weak and broad deep-level emission (DLE) peak, centered at ~2.143 eV, is also seen. Compared with ZnSe nanowires grown by others,[20,21] our MOCVD-grown nanowires show significantly higher intensity in the NBE peak relative to the DLE peak, a testament to their better optical properties. We believe that the strong band-edge luminescence is connected with the low density of dislocations within, as well as the low density of surface defects, as these defects tend to quench the band-edge radiative recombinations. The weakness of the deep-level emissions also suggests that these nanowires are of stoichiometric composition, with perhaps a low density of point defects. The PL spectrum of ZnSe nanorods shows an even stronger relative NBE peak than the nanowires (Fig. 6b). The NBE peak remains at 2.687 eV but the DLE is shifted to lower energy and is at ~2.113 eV. This difference in relative intensities can be accounted for by the smaller surface-to-volume ratio in nanorods than in the nanowires. From our helium temperature cathodoluminescence imaging of individual nanorods (the details of which will be reported in another article), we have identified the surface as the main source of DLE.

In summary, highly oriented arrays of ZnSe nanowires and nanorods were successfully grown by MOCVD on ZnSe epilayers on various GaAs surfaces. When gold was used as a catalyst, growth resulted in round nanowires. Regardless of the surface, the growth direction of the nanowires was always along <110>. When a catalyst was not used, hexagonal nanorods growing along <111> are obtained instead. The nanowires and nanorods were shown by XRD and TEM studies to be single-crystalline zinc blende in structure. We also demonstrated that their orientation on the epilayers could be controlled through epitaxy and choice of the surface of GaAs. The better optical properties and alignment of the resulting nanowires and nanorods make the MOCVD route promising for device applications in nanotechnology.

Experimental

ZnSe epitaxial thin films were grown on GaAs (100), (211)A, and (111)A substrates in a metal–organic chemical vapor deposition (MOCVD) system with a horizontal reactor. The GaAs substrates were steamed in 1,1,1-trichloroethane vapor for 30 min, rinsed with deionized water, and blown dry with N_2 gas just before they were loaded into the MOCVD reactor. Diethylzinc and diisopropylselenide, carried by H_2 at flow rates of 2.8 sccm and 3.6 sccm, were used as precursors, and 7N hydrogen gas was used as the carrier gas. The reactor pressure was kept at 760 torr (101.3 kPa). Substrates were preheated at 600 °C for 20 min in a flowing hydrogen environment prior to the actual growth of ZnSe epilayers at 500 °C. When a catalyst was used, the epilayers were taken out of the reactor and sputter-coated with a very thin layer (~1 nm) of gold, after which they were reloaded into the reactor. For the growth of nanowires, the diethylzinc and diisopropylselenide flow rates were changed to 1.08 sccm and 7.2 sccm, the reactor pressure to 100 torr (13.33 kPa), and the temperature to 550 °C. Their growth times were 1400 s. As for the growth of nanorods, the growth parameters were switched to those of growing nanowires right after the completion of the epilayer.

The synthesized products were characterized by X-ray diffraction (Rigaku RU-300 X-ray rotating anode generator of Cu Kα radiation and Phillips MRD and Huber goniometers); scanning electron microscopy (LEO 1450 VP); and high-resolution transmission electron microscopy (Philips CM 200 microscope operating at 200 kV). Photoluminescence spectra of the synthesized nanostructures were taken at room temperature using the 325 nm line of a He–Cd laser at an output power of 2 mW as the excitation source.

Received: November 18, 2004
Final version: March 3, 2005

[1] a) X. Duan, C. M. Lieber, *Adv. Mater.* **2000**, *12*, 298. b) M. H. Huang, Y. Wu, H. Feick, N. Tran, E. Weber, P. Yang, *Adv. Mater.* **2001**, *13*, 113.
[2] Y. Xia, P. Yang, Y. Sun, Y. Wu, B. Mayers, B. Gates, Y. Yin, F. Kim, H. Yan, *Adv. Mater.* **2003**, *15*, 353.
[3] W. I. Park, G. C. Yi, M. Kim, S. J. Pennycook, *Adv. Mater.* **2002**, *14*, 1841.
[4] M. H. Huang, S. Mao, H. Feick, H. Q. Yan, Y. Wu, H. Kind, E. Weber, R. Russo, P. Yang, *Science* **2001**, *292*, 1897.
[5] L. Cao, Z. Zhang, L. Sun, C. Gao, M. He, Y. Wang, Y. Li, X. Zhang, G. Li, J. Zhang, W. Wang, *Adv. Mater.* **2001**, *13*, 1701.
[6] X. Chen, J. Xu, R. M. Wang, D. P. Yu, *Adv. Mater.* **2003**, *15*, 419.
[7] W. Lee, M. C. Jeng, J. M. Myoung, *Nanotechnology* **2004**, *15*, 254.

ADVANCED MATERIALS

[8] P. Nguyen, H. T. Ng, J. Kong, A. M. Cassell, R. Quinn, J. Li, J. Han, M. McNeil, M. Meyyappan, *Nano Lett.* **2003**, *3*, 925.
[9] X. Chen, J. Xu, R. M. Wang, D. Yu, *Adv. Mater.* **2003**, *15*, 419.
[10] Z. H. Wu, X. Y. Mei, D. Kim, M. Blumin, H. E. Ruda, J. Q. Liu, K. L. Kavanagh, *Appl. Phys. Lett.* **2003**, *83*, 3368.
[11] Y. F. Chen, X. F. Duan, S. K. Chan, I. K. Sou, X. X. Zhang, N. Wang, *Appl. Phys. Lett.* **2003**, *83*, 2665.
[12] K. Hiruma, M. Yazawa, T. Katsuyama, K. Ogawa, K. Haraguchi, M. Koguchi, H. Kakibayashi, *J. Appl. Phys.* **1995**, *77*, 447.
[13] S. Bhunia, T. Kawamura, Y. Watanabe, *Appl. Phys. Lett.* **2003**, *83*, 3371.
[14] X. T. Zhang, Z. Liu, Y. P. Leung, Q. Li, S. K. Hark, *Appl. Phys. Lett.* **2003**, *83*, 5533.
[15] A. M. Andrews, J. S. Speck, A. E. Romanov, M. Bobeth, W. Pompe, *J. Appl. Phys.* **2002**, *91*, 1933.
[16] A. A. Chernov, *Modern Crystallography III: Crystal Growth*, Springer Series in Solid-State Sciences, Vol. 36, Springer, New York **1984**, p. 129.
[17] Y. Ohno, N. Adachi, S. Takeda, *Appl. Phys. Lett.* **2003**, *83*, 54.
[18] R. Beanland, M. Aindow, T. B. Joyce, P. Kidd, M. Lourenco, P. J. Goodhew, *J. Cryst. Growth* **1995**, *149*, 1.
[19] Z. L. Wang, X. Y. Kong, J. M. Zuo, *Phys. Rev. Lett.* **2003**, *91*, 185 502.
[20] B. Xiang, H. Z. Zhang, G. K. Li, F. H. Yang, F. H. Su, R. M. Wang, J. Xu, G. W. Lu, X. C. Sun, Q. Zhao, D. P. Yu, *Appl. Phys. Lett.* **2003**, *82*, 3330.
[21] Y. C. Zhu, Y. Bando, *Chem. Phys. Lett.* **2003**, *377*, 367.

Microscopic Evidence for Spatially Inhomogeneous Charge Trapping in Pentacene**

By *Erik M. Muller* and *John A. Marohn**

The comparatively high mobility of pentacene and its ability to be deposited on flexible substrates at low temperature[1,2] make it an attractive alternative to amorphous silicon in low-cost large-area electronics applications. Potential applications of pentacene thin-film transistors include display drivers, smart cards, and radio-frequency identification tags.[2–4] While pentacene thin-film transistors have exhibited usefully large mobilities (≥ 1 cm^2 V^{-1} s^{-1}) and on–off ratios ($\geq 10^6$),[5] fabricating pentacene transistors with suitable performance for large-scale applications remains a challenge.

In polycrystalline films, mobility is extremely sensitive to processing conditions, being dependent on crystallite size,[6–10] the substrate,[9,10] exposure to oxygen and water,[11,12] and possibly on the purity of the pentacene.[13] Pentacene transistors, particularly on flexible substrates, exhibit undesirably small threshold slopes,[7] and threshold voltages that are too large[2] and which drift due to gate-dependent bias stress.[8] Bottom-contact transistors are likely to be required for low-cost applications yet, in this geometry, making a low-resistance contact between pentacene and a metal is problematic.[14,15]

Microscopic theories of these effects in polycrystalline pentacene—developed to explain the dependence of transistor behavior on time, temperature, or device dimensions—usually invoke charge traps. For example, threshold-voltage shifts have been explained as being the result of a slow structural change in the film that creates deep localized states near the interface.[9] The dependence of the mobility on gate voltage,[1,3,9,10,16,17] temperature,[9] and degree of unintentional doping[17] is usually modeled in terms of the filling of traps. The traps may[10,17,18] or may not[1,9,16] be explicitly associated with grain boundaries, depending on the model. The presumed increase in charge traps at smaller pentacene grains near the electrodes has been used to rationalize the lower apparent mobility in bottom-contact devices.[3]

Despite the apparently central role of charge traps in controlling charge injection and transport, the microscopic origin of charge trapping in polycrystalline pentacene is not known. Trap energies and concentrations have been estimated for pentacene using deep-level transient spectroscopy[19] and space-charge-limited current techniques.[20] Such macroscopic measurements, however, are unable to determine whether charge traps are a bulk phenomenon associated with chemical impurities, or a grain boundary effect, as is generally supposed. To our knowledge, charge traps in pentacene have never been observed microscopically.

In this communication, we use electric force microscopy (EFM) to directly observe and image long-lived trapped charges in a pentacene thin-film transistor as a function of gate voltage. We find that charge traps are distributed inhomogeneously throughout the pentacene film, but, unexpectedly, are not confined solely to grain boundaries. EFM has been used to study pentacene before, but prior work focused on understanding contact resistance by mapping the local potential of an operating thin-film transistor. Nichols et al. showed that contact resistance in a bottom-contact transistor could be controlled by varying the electrode metal[14] while Puntambekar et al. demonstrated that bottom-contact devices were typically contact limited, whereas top-contact devices were not.[15] We use EFM to study charge trapping because, compared to competing techniques, it does not require detailed understanding of the contacts or transport in the bulk.

Pentacene transistors were fabricated with bottom-contact source and drain electrodes recessed into the gate oxide

[*] Prof. J. A. Marohn
Department of Chemistry and Chemical Biology
Cornell University
Ithaca, NY 14853-1301 (USA)
E-mail: jam99@cornell.edu
E. M. Muller
Laboratory of Atomic and Solid State Physics
Cornell University
Ithaca, NY 14853-2501 (USA)

[**] The authors thank Dr. Ricardo Ruiz and Prof. George Malliaras of Cornell University for assistance with pentacene deposition and for many useful discussions. This work was supported by Cornell University, the National Science Foundation (via CAREER award DMR-0134956, the Cornell Nanoscale Science and Technology Facility, and the Cornell Center for Nanoscale Systems, and the Cornell Center for Materials Research).

  DOI: 10.1002/adma.200401174